CI&CEQ
Chemical Industry & Chemical Engineering Quarterly

Available on line at
Association of the Chemical Engineers of Serbia *AChE*
www.ache.org.rs/CICEQ

Chem. Ind. Chem. Eng. Q. 21 (2) 261–268 (2015) CI&CEQ

BORE V. JEGDIĆ[1]
BILJANA M. BOBIĆ[1]
MILOŠ K. PAVLOVIĆ[2]
ANA B. ALIL[3]
SLAVIŠA S. PUTIĆ[4]

[1]Institute of Chemistry, Technology and Metallurgy, University of Belgrade, Belgrade, Serbia
[2]Welding Institute, Belgrade, Serbia
[3]Innovation center, Faculty of Technology and Metallurgy, University of Belgrade, Belgrade, Serbia
[4]Faculty of Technology and Metallurgy, University of Belgrade, Belgrade, Serbia

SCIENTIFIC PAPER

UDC 669.715:620.194.2

DOI 10.2298/CICEQ140324024J

STRESS CORROSION CRACKING RESISTANCE OF ALUMINUM ALLOY 7000 SERIES AFTER TWO-STEP AGING

Article Highlights

- SCC resistance of one-step and new two-step aged Al-Zn-Mg-Cu alloy was tested
- SCC was tested by SSRT and using fracture mechanics method
- After new two-step aging the alloy has considerably higher SCC resistance
- Mechanical properties of one-step aged and new two-step aged alloy are similar
- Two E_a values for process that controls stress corrosion crack rate were obtained

Abstract

The effect of one-step and a new (short) two-step aging process on the resistance to stress corrosion cracking of an aluminum alloy 7000 series was investigated, using slow strain rate test and fracture mechanics method. The aging level in the tested alloy was evaluated by means of scanning electron microscopy and measurements of electrical resistivity. It was shown that the alloy after the new two-step aging is significantly more resistant to stress corrosion cracking. Values of tensile properties and fracture toughness are similar for both thermal states. Processes that take place at the crack tip have been considered. The effect of the testing solution temperature on the crack growth rate on the plateau was determined. Two values of the apparent activation energy were obtained. These values correspond to different processes that control crack growth rate on the plateau at higher and lower temperatures.

Keywords: aluminum alloys, stress corrosion cracking, aging, mechanical properties.

Stress corrosion cracking (SCC) is a time-dependent process that occurs under the influence of residual or imposed tensile stress and specific corrosive environment. Localized corrosion (intergranular, pitting) usually proceeds to SCC. Mechanical damage on the metal surface may play the role of an initial crack [1-3].

Aluminum alloys 7000 series (Al-Zn-Mg-Cu) are characterized by high strength, but they are prone to SCC. However, the tendency of these alloys to SCC changes depending on the content of alloying elements, mechanical, thermal and thermo-mechanical treatment [3-9]. Precipitation hardening of these aluminum alloys takes place through the segregation of GP zones that are transformed through the intermediate η' phase into the equilibrium phase $MgZn_2$ [10--13]. Maximum strength in the aluminum alloys 7000 series is achieved when there is a mixture of GP zones and η' precipitates. In the state of maximum strength, the alloys are prone to SCC and exfoliation corrosion. In the over-aged state, the alloys are characterized with a good resistance towards both SCC and exfoliation corrosion, while in the partially over-aged state the alloys show a slightly lower resistance to SCC and high resistance to exfoliation corrosion [1,10,13,14]. Retrogression and re-aging procedures can be also applied in order to preserve high strength and resistance to SCC [15,16].

The presence of copper in the 7000 series aluminum alloys has a beneficial effect on hardness, increasing the volume fraction of hardening precipitates. It was found that copper is incorporated in GP zones, making them more stable even at higher temperatures [10,17]. In addition, copper atoms replace zinc atoms in the hardening precipitates, particularly at temperatures above 150 °C, making the precipitate nobler [14,17,18].

Correspondence: B.V. Jegdić, Institute of Chemistry, Technology and Metallurgy, University of Belgrade, Njegoševa 12, Belgrade, Serbia.
E-mail: borejegdic@yahoo.com
Paper received: 24 March, 2014
Paper revised: 28 May, 2014
Paper accepted: 8 July, 2014

As it was mentioned above, aluminum alloys 7000 series in the over-aged state (after two-step aging) are characterized by high resistance to SCC and exfoliation corrosion. However, the aging time is relatively long, and hardness of the alloys is significantly reduced (~15% compared to the state of maximum hardness).

The influence of a surrounding environment temperature on the kinetics of the stress corrosion crack growth is of great practical importance, because a large number of SCC processes takes place at increased temperatures. The specific role of copper is not yet fully established for SCC occurrence in aqueous saline solutions, even at room temperature. It was shown that the crack growth rate on the plateau, v_{pl}, at temperatures below 40 °C is highly dependent on the copper content. No copper content dependency was observed at temperatures above 40 °C [19,20].

Based on the results reported [21-25], a shorter two-step aging process can be applied. The new two-step aging process was performed in this work, with shorter aging time. Structural and stress corrosion characteristics of the alloy in the state of maximum hardness as well as in the state after the new two-step aging were investigated in this study. In addition, SCC tests at different temperatures were done in a sodium chloride solution and apparent activation energies were determined.

Examinations of aluminum alloys resistance to SCC have been frequently performed by slow strain rate tests (SSRT) and fracture mechanics tests (FM). Results obtained by SSRT are qualitative in nature, while results obtained by the FM method have a quantitative character.

EXPERIMENTAL

The chemical composition of the tested experimental aluminum alloy is given in Table 1. Test samples were cut from rectangular extruded rods (80 mm×30 mm). The rods were obtained by continuous casting of billets and then subjected to homogenization and extruded.

Heat treatment of the samples was performed according to the following regimes:

- Solution heat treatment at 460 °C/(1 h), quenching in water at room temperature, then artificially aging at 120 °C/(24 h) (one-step aging, indicated in this paper with TA).
- Solution heat treatment at 460 °C/(1 h), quenching in water at room temperature, artificially aging at 100 °C/(5 h), and then at 160 °C/(5 h) (two-step aging, indicated in this paper with TB).

Tensile properties

Tensile properties (tensile strength, R_m, yield strength, $R_{p0.2}$, and elongation, A_5) were determined using short cylindrical proportional specimens ∅ 8 mm (ASTM B557M). Test specimens were made from the alloy in the TA and TB state. The test specimens were cut in transverse direction from pressed rods. Tests were performed using a universal tensile machine Instron.

Micro structural examinations

Micro structural examinations were performed using scanning electron microscopy (SEM Jeol JSM-6610LV). Before SEM analysis, the samples were prepared mechanically and electrochemically. The samples were ground using abrasive papers (1200 to 4000 grit) and polished using diamond paste (5/3 and 3/2 μm). The samples were then electrochemically polished in the perchloric acid ($HClO_4$) and etched in Keller's solution (2 ml HF + 3 ml HCl + 5 ml HNO_3 + 190 ml distillated water) for 10 s.

The presence of intermetallic compounds, their number, size and volume fraction were determined with structural analyzer TAS+, for both thermal states of the alloy (TA and TB).

Electrical resistivity

The measurements of electrical resistivity were performed on the TA and TB samples. The method of measurement is described in ASTM B193 standard. Electrical resistivity was measured by a micro ohmmeter in accordance with the manufacturer's instructions. The value of the measured electrical resistivity (ρ) was recalculated into electrical conductivity ($\chi = 1/\rho$), as well as into the *IACS* (%) factor, using the following equation:

$$IACS = 100\frac{\chi}{\chi_{Cu}} \quad (1)$$

where χ is the value of electrical conductivity of the tested alloy, and χ_{Cu} is the electrical conductivity of pure copper (58.34 MS m^{-1}).

Table 1. Chemical composition of tested aluminum alloy (wt.%)

Zn	Mg	Cu	Mn	Cr	Zr	Fe	Si	Al
7.2	2.15	1.46	0.28	0.16	0.12	0.12	0.05	Rest

Slow strain rate test

The susceptibility of the aluminum alloy to SCC was determined by the SSRT method. The index of tendency to SCC (I_{SCC}) was calculated based on the elongation to fracture during testing of identical samples in the corrosive environment and in the air:

$$I_{SCC} = A_{SCC}/A_0 \quad (2)$$

where A_{SCC} is elongation in the corrosive environment, and A_0 is elongation in the air.

For an alloy resistant to SCC in a given corrosive environment the value of $I_{SCC} \rightarrow 1$, while for an alloy prone to SCC the value of $I_{SCC} \rightarrow 0$.

The SSRT was performed at a chosen value of the initial strain rate from the critical interval of strain rates. Test specimens were of a circular cross section (∅ 6 mm) and of 30 mm working length (ASTM E8). Before the test, dimensions of the specimens were carefully measured. Then, the specimens were degreased in ethanol and placed in the cell for SCC testing. The tests were done using the Instron tensile machine, in the air at the standard initial strain rate and in the corrosive environment (2 wt.% NaCl + 0.5 wt.% Na_2CrO_4, pH 3). In this case, the initial strain rate was 6.94×10^{-6} s^{-1}. The data for the calculation of the I_{SCC} were taken from the obtained stress-strain curve.

Fracture mechanics method

A bolt-loaded double-cantilever-beam (DCB) test specimen was chosen for testing SCC by the FM methodology. The samples were cut in the S-L orientation, since aluminum alloys are most sensitive to SCC at this orientation (force action in the short transverse direction).

The thickness of the sample (B) was calculated based on the known fracture toughness (K_{IC}) and the yield strength ($R_{0.2}$) of the alloy, using the equation:

$$B = \min 2.5\left(\frac{K_{IC}}{R_{p0.2}}\right)^2 \quad (3)$$

Other dimensions of the DCB specimen were determined in dependence on the sample thickness (B = 25 mm). The starting value of the K_{I0} was calculated on the basis of the measured value of the crack length (a), the specimen half-height (H) and the given size of the crack opening on the line of the load (V_Y), according to the following equation (ISO 7539-6):

$$K_{I0} = \frac{EV_Y H\sqrt{3H\left(a+0{,}6H\right)^2+H^3}}{4\left[\left(a+0.6H\right)^3+H^2a\right]} \quad (4)$$

The starting crack was formed mechanically on the specimen [26], and the crack length was precisely measured. The SCC testing was done in accordance with the procedure described [10] in the 3.5 wt.% NaCl solution. The increase of the crack length was measured microscopically in the next 150 days. The diagram of time dependence of the crack length was fitted and smoothed with the appropriate curve. That curve is used for calculating and drawing the diagram of the crack growth rate dependence on the K_I. At the end of testing, a fracture of the samples was performed. On the surface of the fracture, the length of the crack formed mechanically and the total length of the mechanical and stress-corrosion crack were precisely measured. The real value of the stress intensity in the beginning of the SCC test (that approximately corresponds the value of the K_{IC}) and the real value of the stress intensity when the crack practically stops, K_{ISCC}, were calculated (Eq. (4)).

In addition, SCC tests were performed in the 3.5 wt.% NaCl solution at different temperatures, in order to determine the apparent activation energy of the process that controls crack grow rate on the plateau. The length of the crack was measured during the time and the v_{pl} was calculated for every chosen temperature.

RESULTS AND DISCUSSION

Tensile properties

Tensile properties of the alloy in the TA and TB state are given in Table 2. The values of tensile properties are rather high and similar for both thermal states. It can be seen that the value of $R_{p0.2}$ is slightly higher for the thermal state TB, while the values of R_m and A_5 are somewhat higher for the thermal state TA.

Table 2. Tensile properties of tested aluminum alloy

Thermal state	$R_{p0.2}$ / MPa	R_m / MPa	A_5 / %
TA	560	620	10.5
TB	570	600	9.5

Micro structural examinations

The typical microstructure of the alloy (TA and TB state) at low magnification is shown in Figure 1. It can be seen that the alloy is characterized with oriented structure. Grains are elongated and particles of secondary phases are oriented in direction of deformation. There are large light particles and small dark particles of intermetallic compounds of different size. Chemical composition of these particles was determined using SEM/EDS analysis. Typical chem-

ical composition of the intermetallic compounds is presented in Table 3.

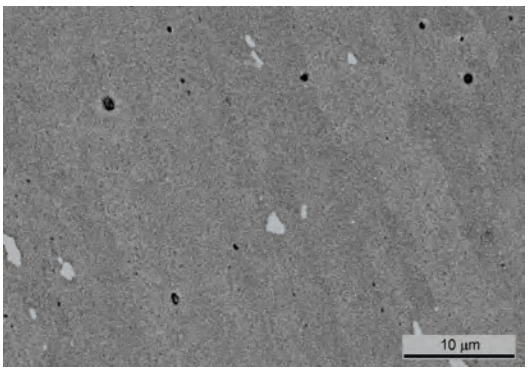

Figure 1. Typical SEM microphotograph of the alloy.

Fracture toughness of the alloy is highly dependent on the size and volume fraction of particles of secondary phases [27,28]. The minimum particle size is 0.67 μm, the maximum particle size is 2.12-2.94 μm, the volume fraction is 2.14 vol.% and the particle number per mm^2 is 7200 for the alloy in TA and TB state.

Microstructures of the alloy after one-step and after two-step aging at higher magnification are shown in Figures 2 and 3. After one-step aging (Figure 2a and 2b) the precipitates are smaller with regard to the precipitates after the two-step aging (Figure 3a and 3b). The mixture of η' phase and stable η phase was formed during the two-step aging (TB). It is possible that most of these precipitates were dissolved in the etching solution. Reduced time of the two-step aging (100 °C/(5 h) + 160 °C/(5 h)) compared to the time of the standard one-step aging (120 °C/(24 h)) can explain the difference in the size of strengthening particles.

Electrical resistivity

Values of the IACS factor change during the second step of two-step aging (TB) as is shown in Table 4.

Table 4. Time dependence of IACS factor for tested aluminum alloy during second step of two-step aging

Time / h	0	4	8	12	16	20	24
IACS / %	31.04	35.92	38.57	40.49	41.43	41.63	41.95

The experimentally obtained results show that the TB state has larger conductivity (36.71% *IACS*) than the TA state (32.56% *IACS*) and the T0 state

Table 3. Typical chemical composition of intermetallic compounds (at.%)

Element	Mg	Al	Si	Cr	Mn	Fe	Cu	Zn
Light particles	0.38	83.5	0.00	0.13	1.32	8.98	2.32	1.72
Dark particles	16.9	65.3	13.7	0.00	0.00	0.00	0.43	1.78

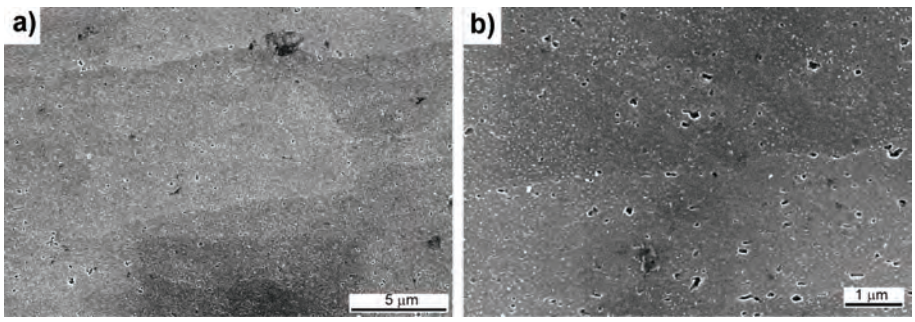

Figure 2. SEM microphotographs of the tested aluminum alloy after one-step aging.

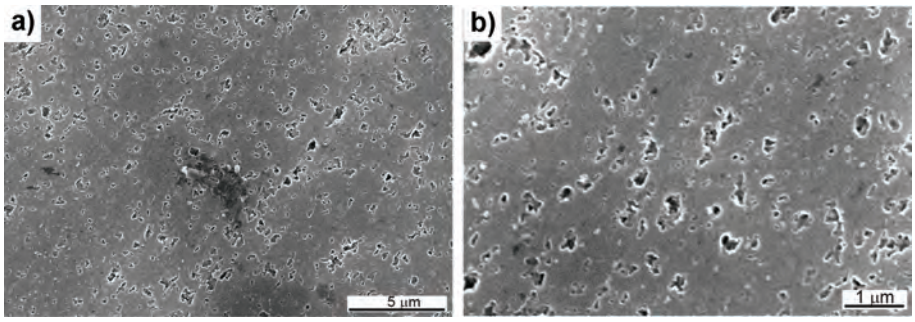

Figure 3. SEM microphotographs of the tested aluminum alloy after two-step aging.

immediately after homogenization annealing (29.65% *IACS*). A supersaturated solid solution with a high concentration of vacancies was obtained after quenching. Fields of elastic strains around vacancies cause significant dissipation of electrons [29], so lower values of conductivity are measured for the thermal state T0. During aging, elastic strains around GP zones and semi coherent η' phase cause electron dissipation to a certain extent (thermal state TA). With appearance of the stable, incoherent η phase during two-step aging, elastic strains decrease, and the alloy conductivity increases. Formed precipitates get coarser and conductivity still increases with a prolonged time of aging (41.95% *IACS*, after 24 h, Table 4). However, mechanical characteristics of the alloy (hardness) are decreased [10], as well as the resistance to SCC and exfoliation corrosion. The resistance to SCC and exfoliation corrosion for aluminum alloys 7000 series was evaluated according to values of electrical conductivity [30]. A detailed model for the electrical conductivity of 7000 aluminum alloys under various aging conditions was presented [31].

Slow strain rate test

The results of SCC testing with SSRT method are presented in Figure 4a. It can be seen that the alloy in the TB state is more resistant to SCC than in the TA state. Index of tendency to stress corrosion cracking I_{SCC} for the alloy after one-step aging is 60.9% and after two-step aging is 98.9%. Processes of crack formation and growth and the final unstable fast fracture are not separated, so the total tendency to stress corrosion cracking is obtained using this method.

A typical experimental stress-strain curve for the alloy in TA state is shown in Figure 4b. Elongation of the specimen in the corrosive environment (NaCl + Na_2CrO_4) is significantly lower compared to the elongation in the air. Index of resistance to SCC for the alloy in TA and TB (I_{SCC}) state was determined from similar diagrams. The results were obtained in a relatively short time (about 10 h per one sample).

Fracture mechanics method

The results of SCC testing by fracture mechanics method are presented in Figure 5, as the dependence of the stress corrosion crack rate on the K_I.

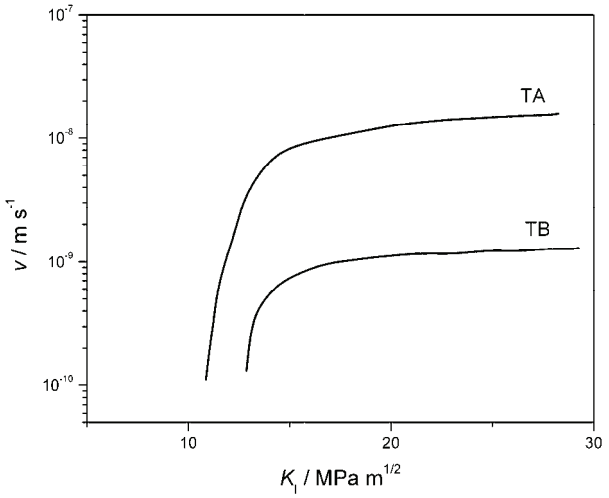

Figure 5. v-K_I dependence for the tested aluminum alloy in TA and TB state.

The value of critical stress intensity factor for stress corrosion crack rate K_{ISCC} is 10.87 MPa $m^{1/2}$ for the alloy in TA state, and 12.87 MPa $m^{1/2}$ for the alloy in TB state. Higher value of K_{ISCC} indicates better resistance to SCC. When the K_I is smaller than the K_{ISCC}, there is no growth of the stress corrosion crack or the growth rate is too small that can be neglected. In the first stadium (steep part of the curve *v*-K_I), the crack growth rate strongly depends on the K_I. In the

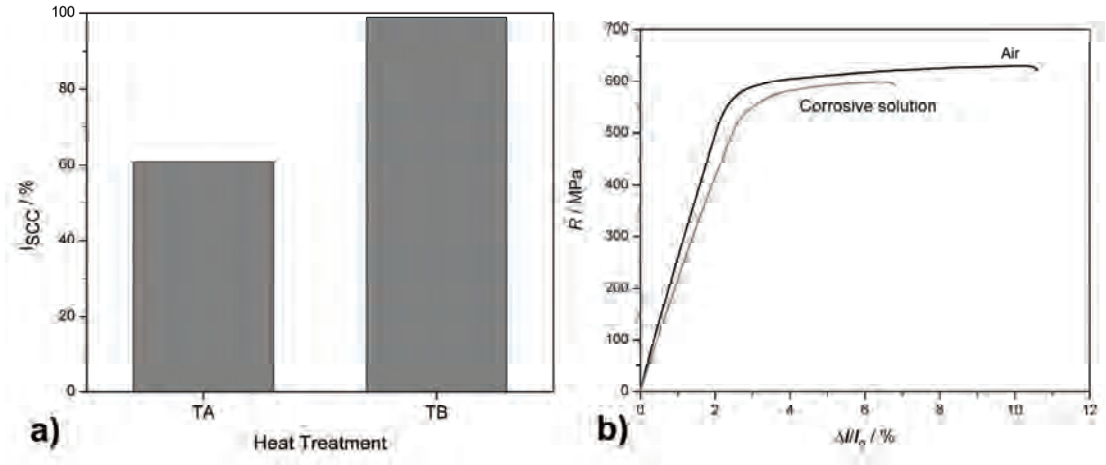

Figure 4. a) I_{SCC} values for the tested aluminum alloy in TA and TB state; b) Experimental stress – strain curve for the alloy in TA state.

second stadium (plateau of the curve v-K_I), the crack growth rate practically does not depend on the K_I. The influence of the alloy heat treatment is significant and it reflects in shifting the level of the second stadium to higher values for the alloy in the thermal state TB (Figure 5). The value of crack propagation rate on the plateau (v_{pl}) is 14.4×10^{-9} m s^{-1} for the thermal state TA, while it is significantly lower for the thermal state TA (1.16×10^{-9} m s^{-1}).

In the beginning of the test the value of the stress intensity factor K_{I0} (that approximately corresponds to the value of K_{IC}) was also determined. The value of K_{I0} for the thermal state TA is 28.25 and 29.25 MPa m$^{1/2}$ for the thermal state TB. It can be seen that fracture toughness of the alloy is somewhat higher after two-step aging than after one-step aging. The size of intermetallic phases and their volume fraction highly influence the fracture toughness of aluminum alloys. Fracture toughness K_{IC} of the tested alloy was calculated according to the model of Hahn and Rosenfield [27,28] using the previously mentioned values for the particle size and volume fraction of the secondary phases. Calculated values of K_{IC} are in good agreement with experimental values.

It can be seen that that the alloy is more resistant to SCC after two-step aging (TB). The difference in SCC resistance is highly reflected on the value of the crack propagation rate on the plateau v_{pl} (Figure 5). The value of the v_{pl} is lower for more than one order of magnitude for the TB state. The structure of the tested alloy after two-step aging is considerably more resistant to SCC than the structure after one-step aging. The maximum strength of the alloy (TA state) is obtained when GP zones and η' precipitates are present in the alloy structure. Local plastic deformation at the tip of the stress corrosion crack causes mainly planar slipping when dislocations cut GP zones and smaller particles of η' phase. It comes to the accumulation of dislocations at grain boundaries at the crack tip, which causes increase in local stress, so that SCC starts at lower external stress. This creates favorable conditions for SCC to occur according to the mechanism of local hydrogen embrittlement or to the mechanism of anodic dissolution.

In the TB state, a great number of GP zones is created in the first step, at lower aging temperature (100 °C). During the second step of aging (160 °C) particles of η' phase are precipitated on GP zones, where they are partially transformed into the stable η phase. In this case, the local plastic deformation at the crack tip is homogeneous. Dislocations cannot succeed in cutting particles of the stable η phase and due to this the dislocations are uniformly distributed inside the grains. There is no local increase in stress at the grain boundaries, which has a favorable influence to SCC resistance. The presence of the stabile η phase in the thermal state TB has no significant influence on the values of mechanical properties of the alloy (Table 2). Duration of the two-step aging performed in this work (Experimental part) was shorter compared to the time of the standard one-step and standard two-step aging. The values of tensile properties and fracture toughness are similar for the alloy in both thermal states (TA and TB).

Tested aluminum alloy contains 1.46 wt.% Cu (Table 1). Alloying with copper reflects in the electrochemical characteristics of the alloy. In the Al-Zn--Mg alloys, the η phase precipitated on the grain boundary is anodic compared to the grain itself (which is covered with a passive film). These conditions are favorable for intergranular corrosion and SCC to occur. In the tested alloy, copper atoms enter into the solid solution and into the $Mg(AlCuZn)_2$ precipitates, making them nobler [14,17,18]. The precipitates on the grain boundaries are dissolved slower, and the cathodic reaction (hydrogen ion reduction) becomes more difficult [10,14]. In the presence of copper, GP zones are more stable at higher temperatures and the fraction of the strengthening precipitates in the alloy increases. This results in the increase in strength and resistance to SCC [10,17,18]. Accordingly, copper affects the mechanism of plastic deformation (slipping) and the electrochemical characteristics of the solid solution and precipitates. The influence of other factors, such as formation of magnesium hydride at grain boundaries [11,32-35] and other possible mechanisms of SCC occurrence are not considered in this paper.

The influence of the test solution temperature on the v_{pl} is shown in Fig. 6. The exponential increase of the v_{pl} with the increase in temperature was noticed, which is expressed by the following equation:

$$v = v_0 \exp(-E_a/RT) \quad (5)$$

where E_a is the apparent activation energy of the process that controls the v_{pl}.

If the previous equation is logarithmed, a linear dependence between the logarithm of the v_{pl} and the reciprocal value of the temperature is gained:

$$\ln v = \ln v_0 - E_a/RT \quad (6)$$

The dependence of the v_{pl} on the reciprocal value of the temperature is shown in Figure 6. From the slope of the straight line, the apparent activation energy of the process that controls the v_{pl} is obtained. There are two values of the apparent activation energy. One value (E_a = 46.6 kJ mol^{-1}) refers to the temperature interval from 23 to 83 °C, while the other

(E_a = 70.4 kJ mol^{-1}) refers to the lower testing temperatures, from 3 to 23 °C. These values of apparent activation energies correspond to different processes that control the v_{pl}. This is in accordance with the reported results [10,19].

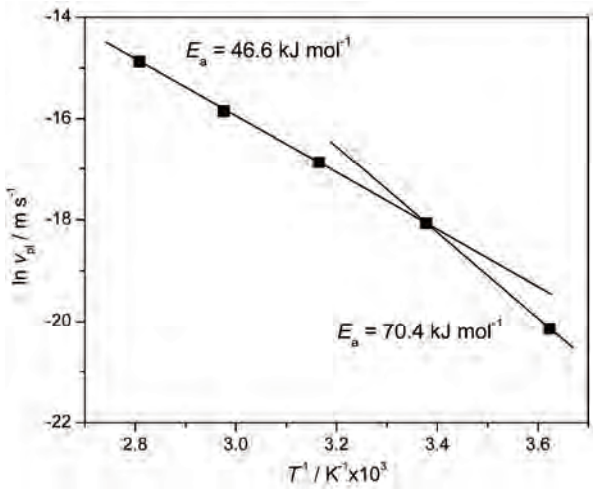

Figure 6. Temperature dependence of v_{pl} during SCC testing (TA state).

According to [19,20] crack propagation rate on plateau, v_{pl}, at temperatures above 40 °C is associated with aluminum hydride formation. The decomposition of aluminum hydride within the crack-tip region leads to significantly enhanced local entry of hydrogen, which facilitates the observed increase of v_{pl}, independent of the copper content. Crack propagation rate on plateau at temperatures below 40 °C is dependent on the availability of hydrogen generated *via* the electrochemical process. Anodic dissolution and grain boundary slipping are possible candidates for occurrence of SCC processes at temperatures below 40 °C.

CONCLUSIONS

Resistance to SCC of a high strength 7000 series aluminum alloy was tested. The alloy after the new two-step aging shows considerably higher resistance to SCC compared to the alloy after one-step aging. The values of tensile properties and fracture toughness are similar for both thermal states. Duration of the two-step aging was very short.

The results obtained by the SSRT method indicate total resistance of the alloy to SCC. It was shown that the thermal state TB is more resistant to the SCC than the thermal state TA. The value of I_{SCC} is 98.9% for the thermal state TB and 60.9% for the thermal state TA. The value of K_{ISCC} is higher for thermal state TB (12.87 MPa m$^{1/2}$) compared to thermal state TA (10.87 MPa m$^{1/2}$). The value of v_{pl} is lower for more than one order of magnitude for the two-step aged alloy (1.16×10^{-9} compared to 14.4×10^{-9} m s^{-1} for the thermal state TA). Two values of apparent activation energy for the process that controls the v_{pl} were obtained.

Acknowledgement

This work was co-financed from the Ministry of Education, Science and Technological Development of the Republic of Serbia through projects TR 34028 and TR 34016.

REFERENCES

[1] H.R. Jones, in Corrosion: Fundamentals, Testing, and Protection, Vol 13A, D.S. Cramer, B.S. Covino, Ed., ASM International, Materials Park, OH, 2003, p. 346

[2] D. Landolt, Corrosion and Surface Chemistry of Metals, EPFL Press, Lausanne, 2007, p. 491

[3] W.R. Herberg, Deformation and Fracture Mechanics of Engineering Materials, John Wiley. and Sons, New York,, 1983, p. 329

[4] O.M. Speidel, Metall. Mater. Trans., A **6** (1975) 631-651

[5] F.B. Brown, Stress Corrosion Cracking Control Measures, NACE monography 156, NACE, Houston, TX, 1977, p. 23

[6] J. Moran, in Corrosion: Fundamentals, Testing, and Protection, Vol 13A, D.S. Cramer, B.S. Covino, Ed., ASM International, Materials Park, OH, 2003, p. 275

[7] S.G. Peng, H.K. Chen, Y.S. Chen, C.H. Fang, Mater. Corros. **63** (2012) 254-258

[8] J. Onoro, Mater. Corros. **61** (2010) 125-129

[9] S.C. Paglia, V.K. Jata, G.R. Buchheit, Mater. Corros. **58** (2007) 737-750

[10] W.A. Thompson, M.I. Bernstein, in Advances in Corrosion Science and Technology, Vol 7, G.M. Fontana, W.R. Staehle, Ed., Plenum Press, New York, 1980, p. 53

[11] M. Bobby, P. Kannan, S. Bala, S.V. Raja, in Stress Corrosion Cracking, Theory and Practice, S.V. Raja, T. Shoji, Ed., Woodhead Publishing, Oxford, 2011, p. 307

[12] S.V. Sinjavskij, D.V. Valjkov, D.V. Kalinin, in Corrosion and Protection of Aluminium Alloys, Metalurgija, Moskva, 1986, p. 43

[13] B.V. Jegdić, Sci.-Tech. Rev. **13** (2003) 19-24

[14] T.J. Summerson, D.O. Sprowls, in: Aluminum Alloys, their Physical and Mechanical Properties, EMAS, Cradley Heath, 1986, p. 1576

[15] Y.P. Xiao, Q.L. Pan, W.B. Li, X.Y. Liu, Y.B. He, Mater. Des. **32** (2011) 2149-2156

[16] M. Angappan, V. Sampath, B. Ashok, V.P. Deepkumar, Mater. Des. **32** (2011) 4050-4053

[17] E.J. Hatch, Aluminum: Properties and Physical Metallurgy, ASM International, Materials Park, OH, 1984, p. 242

[18] F.L. Mondolfo, Aluminum Alloys: Structure and Properties, Butterworths, London, 1976, p. 842
[19] N.J. Henry Holroyd, M.G. Scamans, Metall. Mater. Trans., A **42** (2011) 3979-3998
[20] N.J. Henry Holroyd, G.M. Scamans, Metall. Mater. Trans., A **44** (2013) 1230-1253
[21] G. Sha, A. Cerezo, Acta Mater. **52** (2004) 4503-4516
[22] G. Sha, A. Cerezo, Acta Mater. **53** (2005) 907-917
[23] L.B. Ou, G.J. Yang, Y.M. Wei, Metall. Mater. Trans., A **38** (2007) 1760-1773
[24] T. Marlaud, A. Deschamps, F. Bley, W. Lefebvre, B. Baroux, Acta Mater. **58** (2010) 248-260
[25] P.S. Lynch, Metall. Mater. Trans., A **44** (2013) 1209-1229
[26] B. Phull, in Corrosion: Fundamentals, Testing, and Protection, Vol 13A, D.S. Cramer, B.S. Covino, Ed., ASM International, Materials Park, OH, 2003, p. 575
[27] G.T. Hahn, A.R. Rosenfield, Metall. Mater. Trans., A **6** (1975) 635-668
[28] R.H. Van Stone, J.A. Psioda, Metall. Mater. Trans., A **6** (1975) 668-670.
[29] I.I. Novikov, Theory of Heat Treatment of Metals, Mir Publishers, Moscow, 1978, p. 298
[30] J.R. Davis, Corrosion of Aluminum and Aluminum Alloys, ASM International, Materials Park, OH, 1999, p. 99
[31] J.M. Starink, M.X. Li, Metall. Mater. Trans., A **34** (2003) 899-911
[32] A.G. Young, R.J. Scully, Metall. Mater. Trans., A **33** (2002) 101-115.
[33] R.K. Cooper, G.R. Kelly, Corros. Sci. **49** (2007) 2636--2662
[34] G.R. Song, K.M. Tseng, J.B. Zhang, J Liu, H.Z. Jin, S.K. Shin, Acta Mater. **44** (1996) 3241-3248
[35] D.T. Burleigh, Corrosion **47** (1991) 89-97.

BORE V. JEGDIĆ[1]
BILJANA M. BOBIĆ[1]
MILOŠ K. PAVLOVIĆ[2]
ANA B. ALIL[3]
SLAVIŠA S. PUTIĆ[4]

[1]Institut za hemiju, tehnologiju I metalurgiju, Univerzitet u Beogradu, Beograd
[2]Institut za zavarivanje, Beograd
[3]Inovacioni centar Tehnološko-metalurškog fakulteta, Beograd
[4]Tehnološko-metalurški fakultet, Univerzitet u Beogradu, Beograd

NAUČNI RAD

OTPORNOST ALUMINIJUMSKE LEGURE SERIJE 7000 PREMA NAPONSKOJ KOROZIJI POSLE DVOSTEPENOG TERMIČKOG TALOŽENJA

Ispitivan je uticaj jednostepenog i novog (kratkotrajnog) dvostepenog termičkog taloženja na otpornost prema naponskoj koroziji aluminijumske legure serije 7000, primenom metode male brzine deformacije i metode mehanike loma. Stepen starenja ispitivane legure je procenjen primenom skening elektronske mikroskopije i na osnovu merenja električne otpornosti. Pokazano je da je legura posle novog dvostepenog termičkog starenja znatno otpornija prema naponskoj koroziji. Vrednosti zateznih karakteristika i žilavosti loma su slične za oba termička stanja legure. Razmatrani su procesi koji se odvijaju na vrhu naponsko-korozione prsline. Određen je uticaj temperature rastvora za ispitivanje na brzinu rasta prsline na platou. Određene su dve vrednosti prividne energije aktivacije. Ove vrednosti odgovaraju različitim procesima koji kontrolišu brzinu rasta prsline na platou, na visokim i niskim temperaturama.

Ključne reči: aluminijumske legure, naponska korozija, starenje, mehaničke osobine.